Numerical modeling of stress state and displacement characterization around an UCG-induced cavity of coal seam VI of Barapukuria Coal Deposit, NW Bangladesh

Md. Rafiqul Islam[1]*, Md. Abdul Hye[2] and **Mohammed Omar Faruque [1]**

Abstract- In this paper, FEM numerical modeling is used to simulate stress patterns and displacement around an UCG-induced cavity associated with coal seam VI and overburden thickness of about 336 m of the Barapukuria coal deposit in northwest Bangladesh. We simulated in-situ stress patterns around UCG-induced cavity, displacement characterization and failure tendency of rock strata in terms of strength factor. Modeling results reveal that the maximum value of the major principal stress (σ_1) is about 56.90 MPa at the bottom of the coal pillar, whereas the minimum values of major principal stress range from 4.05 to 7.10 MPa. The maximum values of major principal stress are highly concentrated in and around the coal pillar rather than that of roof and floor of the cavity. The maximum values of total displacement and vertical displacement associated with the width and height of the cavity imply that the lateral growth will sustain for a rational time, which will enhance the long life of a gasifier. Simulated strength factor at the immediate roof of the cavity implies that the overburden strata strength is good enough to enhance the lateral growth of a gasifier and facilitate the more cost-effective operation.

Keywords: *Coal Seam VI, Underground Coal Gasification, Cavity, Principal Stresses, Displacement, Barapukuria coal deposit*

1. INTRODUCTION

UNDERGROUND coal gasification (UCG) is a promising technology for the utilization of un-mined coal seams associated with the low grade and inaccessible coal resources. UCG technology is better for utilizing the coal resources from the thin seams, deep seams, coal seams under water, or coal with high contents of sulphur, ash, and methane, which are difficult, unsafe, or uneconomic to exploit using traditional mining methods. It is a combination of development, mining, and gasification. It has environmental and other advantages over the conventional mining process. UCG includes higher coal resource recovery rate, better economic performance, higher utilization ratio, increased worker safety, and it is more friendly to the environment [1,2]. UCG permits coal to be gasified in situ within the coal seam, via a matrix of wells. In this system, coal is ignited and air is injected underground to sustain a fire, which is essentially used to "mine" the coal and produce a combustible synthetic gas [3]. During the UCG process, usually, a panel (cavity) is formed throughout the coal seam. The burning coal seam as well as country rocks in the vicinity of a UCG panel are subjected to high temperatures. The temperature from burning of the coal in the cavity is usually in the range of 700–900°C, but it may reach up to 1200°C. UCG operation imposes significant geomechanical changes to the strata [4, 5, 3, 6] that may cause stress redistribution in the vicinity of an UCG cavity. In underground coal gasification, the immediate roof strata not only undergo displacement and deformation but also change their mechanical properties and aggregate state. Displacement in roof strata results in a loss of integrity of the underground UCG gasifier cavity, increased losses of oxygen supply (injected air) and gasifier gas losses, and a heat loss to the surrounding strata that can disrupt the entire UCG plant process [7]. Therefore, understanding the stress state and strata displacement around an UCG-induced cavity (panel) is an important part before application of UCG technology. In order to understand the stress distribution and displacement around an UCG cavity-induced country rocks, finite element method (FEM) numerical modeling can provide a comprehensive results. In the present study, coal seam No. VI, around the Borehole No. DOB#4 (Deep Observation Borehole) of the Barapukuria coal deposit of northwest Bangladesh has been considered as a case study to understand the stress distribution and displacement behavior around an UCG-induced cavity.

2. A COAL SEAM SUITABILITY FOR UCG

A coal seam suitable for UCG was proposed by different authors [8, 9, 10, 11, 12, 13, 14, 15, 16]. The criteria of coal seam suitability for UCG are the results of gathered information concerning geological, technical and hydrogeological specifics [17]. The main geological factors that should be considered in UCG system are: (i) coal thickness,(ii) coal rank, quality, and internal structure of the seam (seam continuity, barren partings etc.), (iii) overburden lithology and thickness, (iv) tectonic features of the coal deposit, and (v) hydrogeology of the coal deposit and its environment [16]. According to Ergo Exergy, four important geological parameters that must be required for underground coal gasification project are as follows-

- Coal seam thickness from 0.5 to 30 m,
- Coal seam dip from 0^o to 70^o,
- Overburden depth from 30 to 800 m, and

[1] Department of Petroleum & Mining Engineering, Shahjalal University of Science & Technology (SUST), Sylhet 3114, Bangladesh.
[2]Department of Mathematics, Shahjalal University of Science & Technology (SUST), Sylhet 3114, Bangladesh.
*Corresponding author. Tel.: +8801749611336
E-mail address: dmrislam74@gmail.com (Dr. M.R. Islam).

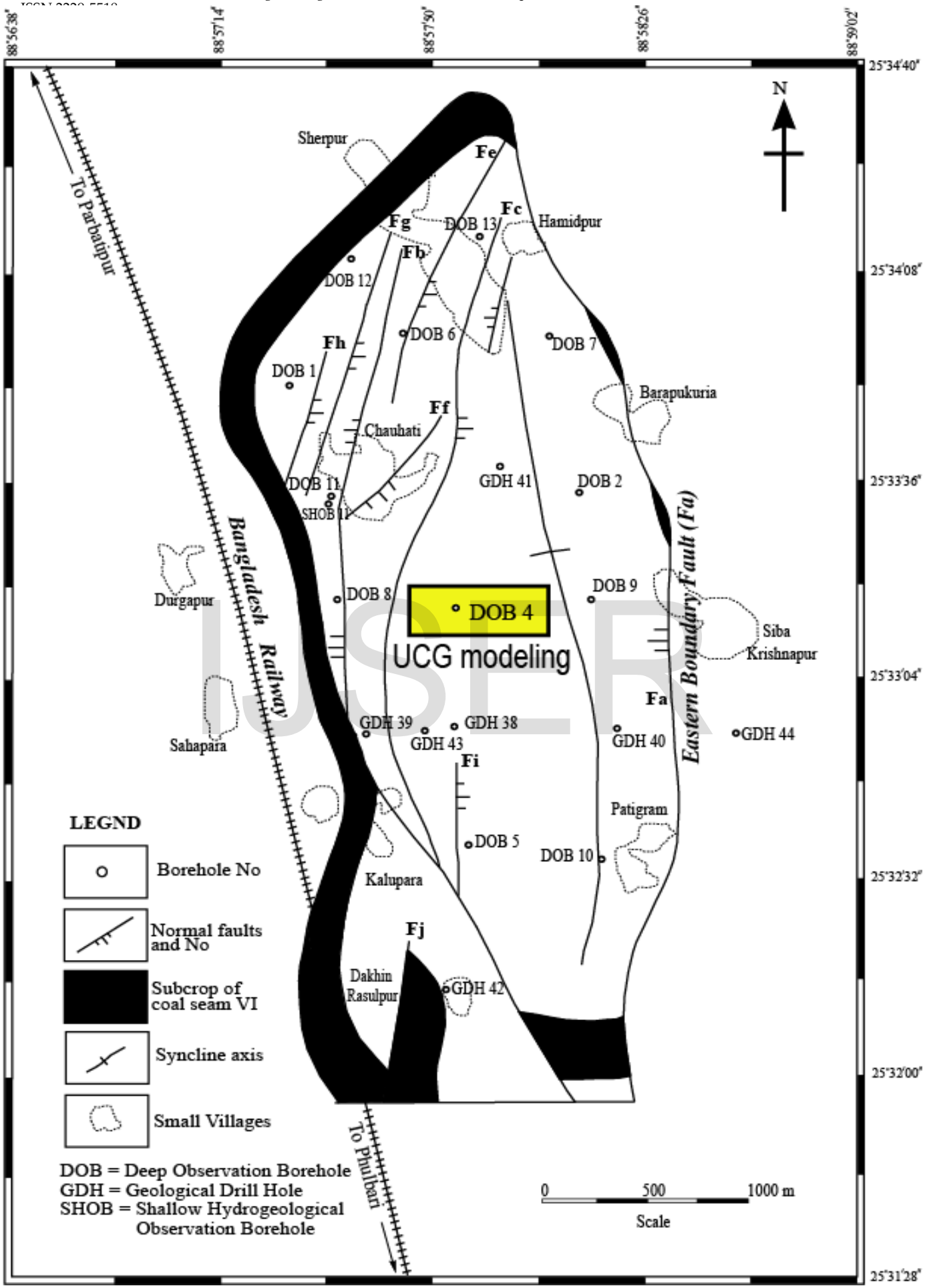

Figure 1. Borehole location of DOB4 in the plan view the Barapukuria Coal Deposit, NW Bangladesh (after Islam and Hayashi, 2008)

- Calorific value (LHV) of coal from 8.0 to 30 MJ/kg (which includes low-quality Lignite to Bituminous coal)(http://www.ergoexergy.com/eucg.htm).

All parameters, as mentioned above, match the Barapukuria coal deposit for UCG project very well. The Barapukuria coal basin is totally concealed by an unconformable cover of between 100–220 m Dupi Tila Formation. The sequence is correlated into four formations on the basis of age and lithology, like (i) Quaternary Madhupur clay, (ii) Late Miocene/Pliocene Dupi Tila (upper and lower), (iii) Permian Gondwana Group and (iv) Pre-Cambrian Archaean Basement. The stratigraphic depth of coal seam VI around the DOB#4 borehole is ranged from 336 to 372 m, seam thickness 36 m, angle of inclination is 0^o to 10^o. The thickest and most laterally extensive seam of the Barapukuria deposit is designated Seam VI, with an average thickness of about 36 m. The general structure of the basin is of an asymmetrical faulted syncline with an approximately N-S axis. The Permian Gondwana coal-bearing sediments within the syncline rest unconformably on the metamorphic Archaean (Precambrian) basement complex. This sequence is up to 390 m in thickness, and comprises predominantly continental arenaceous sediments, with subordinate siltstones, shales and up to six coal seams [18, 19, 20, 21, 22, 23]. Tectonic faults within the Barapukuria coal basin are divided into two systems: (1) intra-basinal faults, and (2) boundary faults. There are 37 intra-basinal faults within the basin, which have an estimated vertical resolution of about 10 m.

The Eastern Boundary Fault (Fig. 1) striking NNW-SSE over at least 5 km has controlled sedimentation within the basin. The fault is down thrown to the west and affects formations from the basement to the Tertiary. The fault plane dips at 70–75° towards the west with an estimated vertical displacement of more than 200 m with a dominant dip-slip component [19, 24].

The Barapukuria coal is high volatile B bituminous rank. From proximate analysis of Seam VI, volatile matter varies between 25.8 and 33.1% (db) and from 34 to 40% (dmmf). Calorific value varies between 5546 and 7202 (kcal/kg). Average ash content (dry basis) volatile matter, and fixed carbon for Seam VI are 16.37%, 30.27%, and 53.36%, respectively, although these vary within different zones of the seam. Ultimate analyses (dry ash free basis) indicate that typical contents of total carbon, hydrogen, nitrogen, oxygen, and sulphur are 83.21%, 4.98%, 1.68%, 9.48%, and 0.64% respectively [19, 24].

The hydrogeology of the Barapukuria coal deposit is as follows:

- The Upper Dupi Tila aquifer is a prolific groundwater reservoir extending all over larger areas of Bangladesh.
- The Gondwana Sandstone is a poor aquifer, but is in hydraulic connection with the Upper Dupi Tila aquifer in the northern part of the deposit where the Lower Dupi Tila aquiclude is absent.

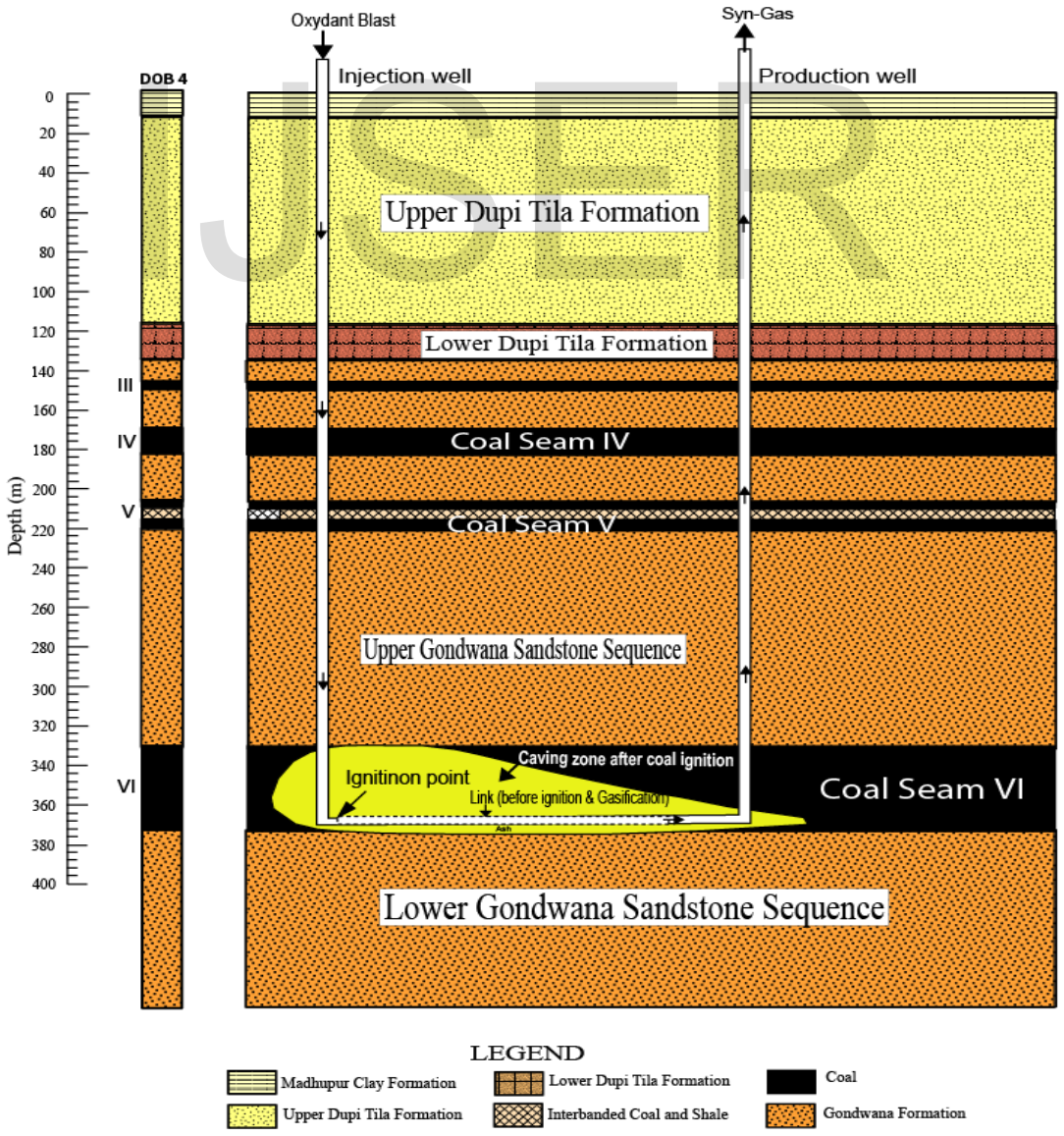

Figure 2. Schematic view of caving zone associated with FEM numerical modeling Underground Coal Gasification (UCG) of Seam No. VI of Barapukuria Coal Deposit, NW Bangladesh

- All Gondwana sandstones are typically jointed, although the joints are frequently mineralised or infilled which reduces the secondary permeability of the aquifer. There appears to be a moderate dynamic balance between the Upper Dupi Tila aquifer and the underlying Gondwana, with an almost flat hydraulic gradient (0.0004–0.0006). Average transmissivity, specific yield, storage coefficient, and velocities were 1200 m^2/day, 25% to 30%, 0.0004, and 0.02 m/day respectively [19, 24].
- The porosity of the overburden and the interbedded Gondwana strata varies from 23.90% for very fine-grained sandstone to 33.3% for clays. The Upper Dupi Tila aquifer has a mean porosity of 33%. In the Lower Dupi Tila, with predominantly clayey sands, the porosity is about 41%. In Gondwana sandstones, the average porosity is about 20% [19, 24]. The calculated porosity of coal ranges from 1.6% to 3.2% [19].
- The permeability of the various lithologies ranges from 3.67 to 75 mD, and 4.81 to 558 mD for medium, and coarse grained sandstone, respectively. The upper coal seams have a permeability between 9.8 mD and 137.8 mD because these seams are comparatively soft and to a varying extent are in hydraulic continuity with the Upper Dupi Tila aquifer. Seam VI has a permeability range from 13 mD to 119 mD [19, 24].

3. MODEL GEOMETRY AND BOUNDARY CONDITIONS

We used Finite Element Method (FEM) numerical modeling, which emphasizes the distribution contours of principal stresses (σ_1 and σ_3) that lead to the failure of the rock surrounding the cavity associated with underground coal gasification. We also attempted to appraise the deformation around the caving. We applied the software package R.S2.9 to analyze the stress distribution and the deformation of the surrounding rock mass of UCG-induced caving. A model (Fig. 2) was constructed that incorporates the location of UCG-induced caving, according to plane strain conditions. The model considers a vertical section based on DOB#4 borehole of the Barapukuria coal deposit corresponding to an overburden thickness of about 336 m. The geometry of the model is simple and consists mainly of six domains associated with coal seams and rocks corresponding to an overburden thickness of about 336 m. The present numerical model accounts for both coal seams III, IV, V and VI and the overburden rocks strata with a bed rock stratum. The imposed mechanical rock parameters are shown in Table 1. Two parallel cavings were modeled with 250 m in width and 36 m thick of ignition height around the injection well. The width of coal pillar between two caving zones is about 50 m. A Mohr-Coulomb failure criterion was adopted with rock mechanics parameters (Table 1). Model geometry, mesh and boundary conditions are shown in Fig. 3. With regard to the stress analysis boundary conditions, the upper surface of the model is almost free and two corners are restrained by both axes (X, Y). The left and right hand sides of the model and the bottom are restrained by both axes (X, Y).

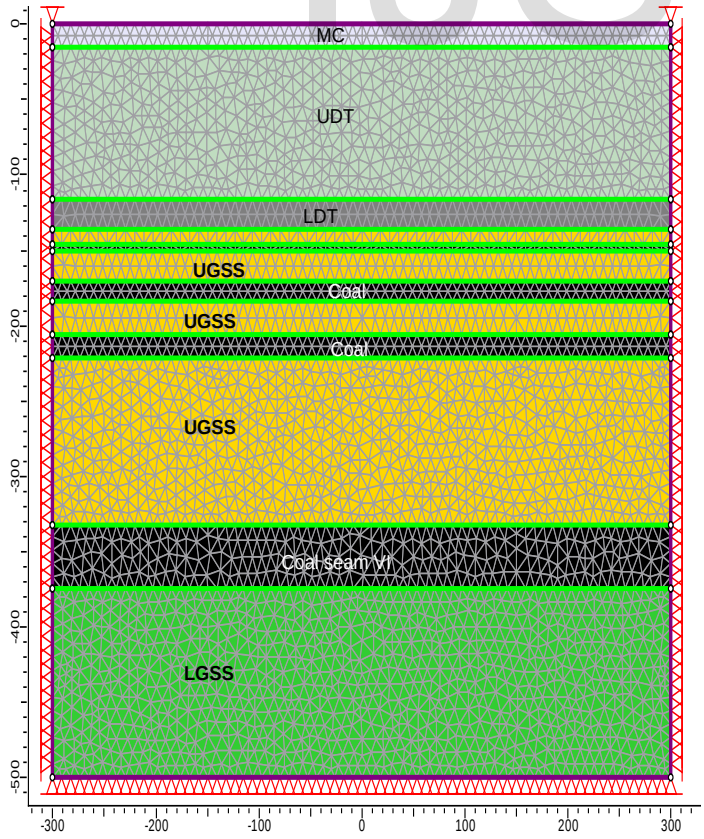

Figure 3. Model mesh and boundary condition before ignition and generation of caving zone. MC = Madhupur Clay; UDT = Upper Dupi Tila; LDT = Lower Dupi Tila; UGSS = Upper Gondwana Sandstone Sequence; LGSS = Lower Gondwana Sandstone Sequence

Table 1. Rock mechanical properties of geological formations of the Barapukuria coal deposit, northwest Bangladesh.

Rock mechanical properties	MC	UDT	LDT	UGSS	Coal	LGSS
Tensile strength (peak) (MPa)	0	400	0	4000	500	4000
Friction angle (peak) (deg.)	20	35	23	30	28	30
Cohesion (peak) (MPa)	25	500	30	7000	5000	7000
Unit weight (MN/m^3)	0.018	0.021	0.020	0.025	0.020	0.025
Youngs modulus (MPa)	10	150	100	250	15	250

Abbreviations: MC = Madhupur Clay; UDT = Upper Dupi Tila; LDT = Lower Dupi Tila; UGSS = Upper Gondwana Sandstone Sequence; LGSS = Lower Gondwana Sandstone Sequence.

4. GOVERNING MATHEMATICAL EQUATIONS

The governing mathematical equations that have been used in the present numerical simulation are referred to Appendix section.

5. MODEL RESULTS

Numerical modeling results are illustrated in Fig. 4, Fig. 5, Fig. 6. The modeling results are presented in terms of three rock mechanical parameters as follows- (i) principal stresses (σ_1 and σ_3) and differential stress, (ii) displacement values and (iii) strength factor around the caving zone. Fig. 4ab shows the distribution contours of the σ_1 and σ_3 stresses. The maximum value of σ_1 stress in our model is about 56.90 MPa at the bottom of the coal pillar, which is located between the two caving zones after ignition. The stress contours are highly concentrated around this portion of the coal pillar (Fig. 4a). The stress is higher near the upper end of the coal pillar at about 19.30 MPa. The minimum values of σ_1 stress at the middle upper part of the caving is from 4.05 to 7.10 MPa and at the bottom of the caving is 7.10 MPa (Fig. 4a).

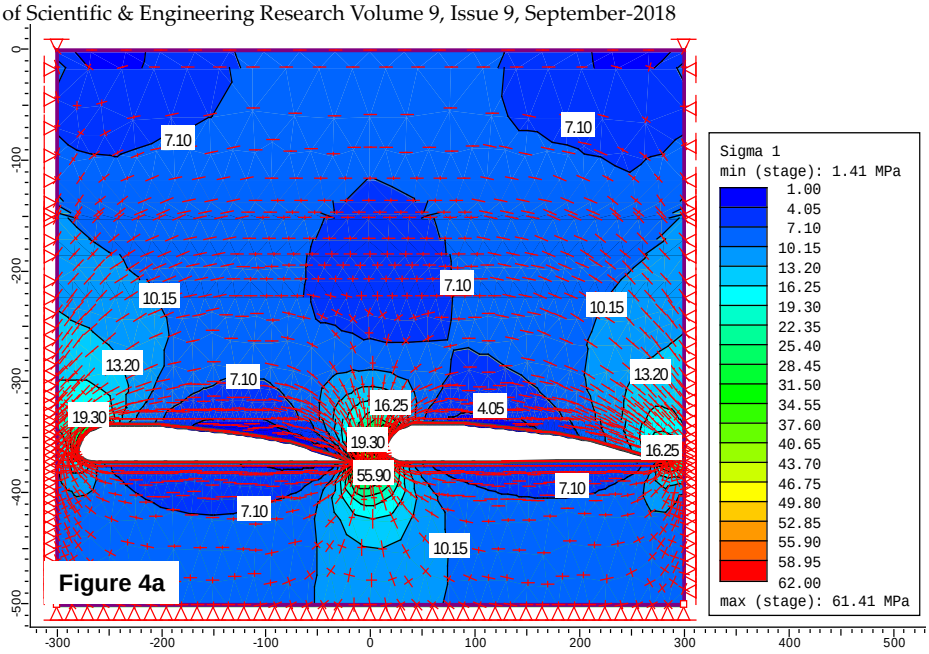

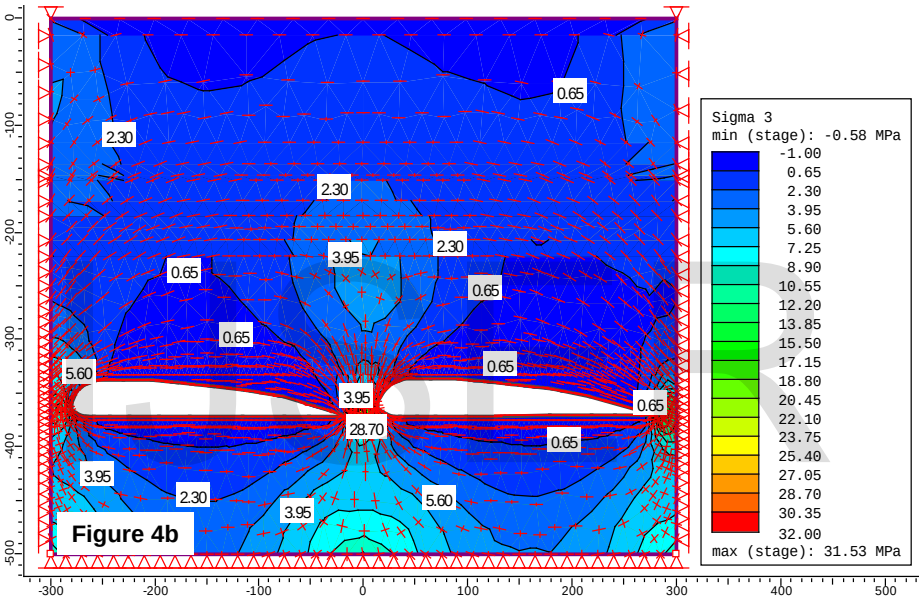

Figure 4 ab. Distribution contours of σ1 and σ3 after development of caving zone due to ignition

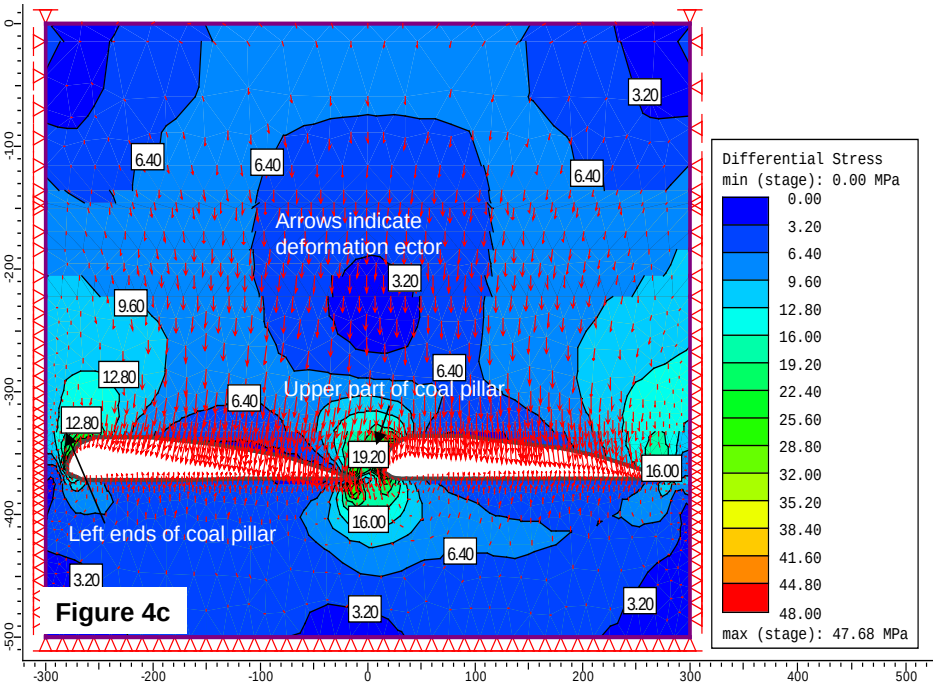

Figure 4c. Distribution contours of differential stress after development of caving zone due to ignition

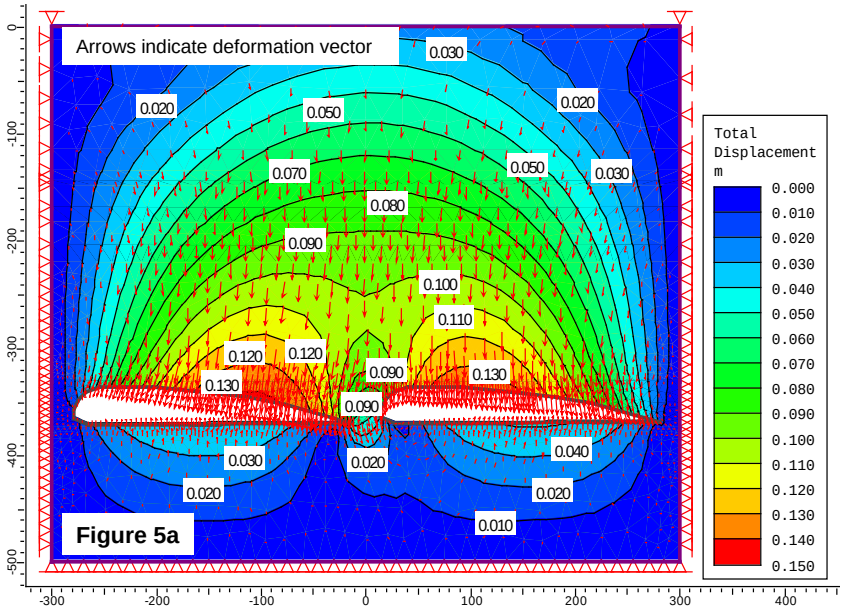

Figure 5a. Distribution contours of total displacement (m) after development of caving zone due to ignition

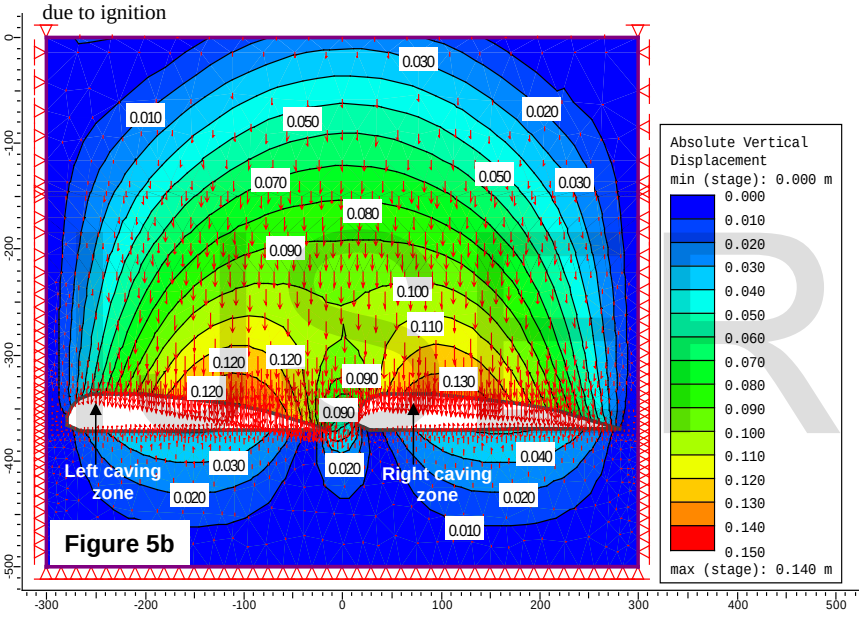

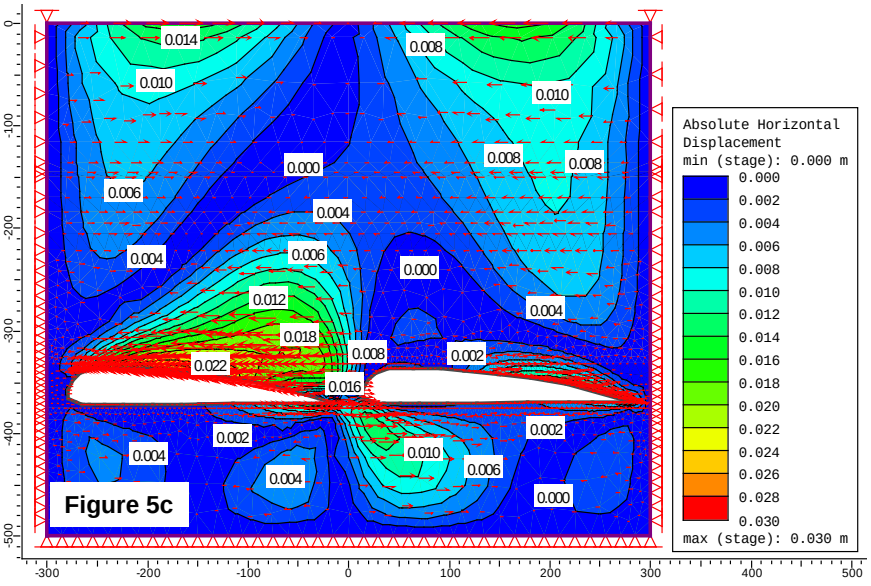

Figure 5bc. Distribution contours of absolute vertical displacement and absolute horizontal displacement after development of caving zone due to ignition

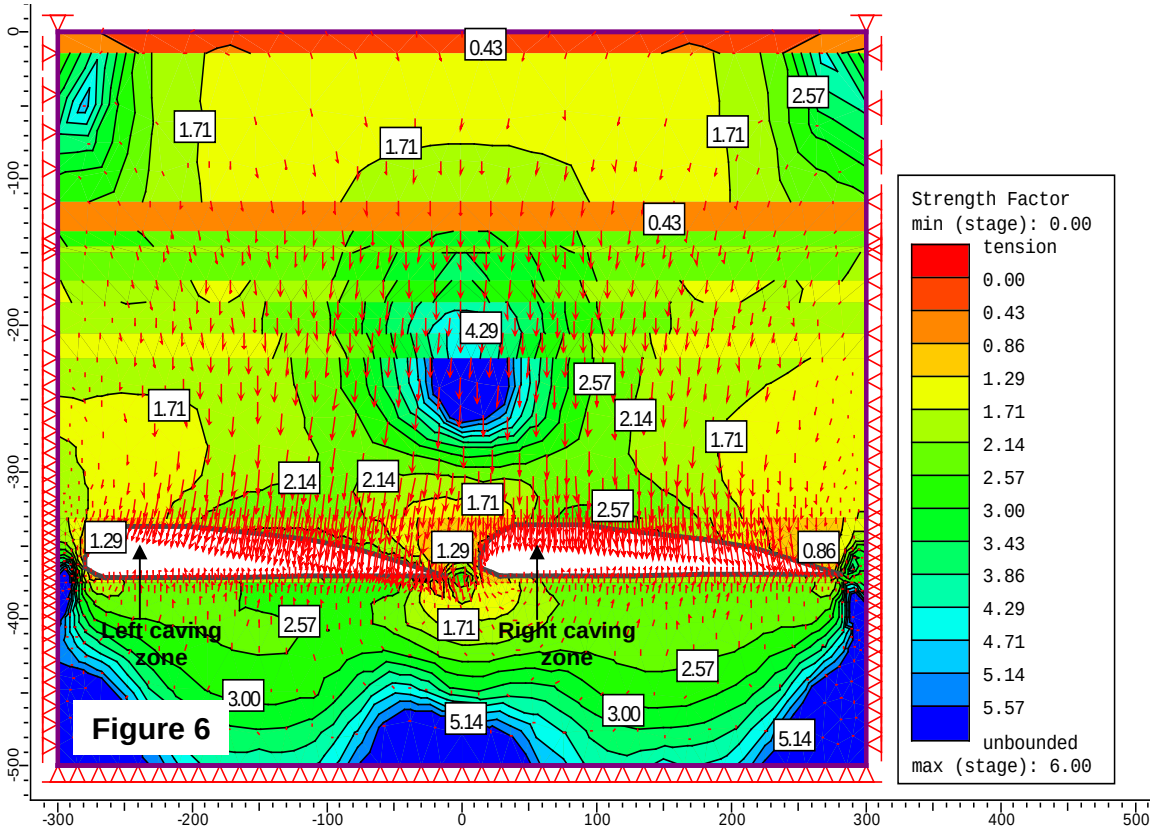

Figure 6. Distribution contours of strength factor after development of caving zone due to ignition

The distribution of the σ_3 stress is shown in Fig. 4b. The stress is higher near the bottom of the coal pillar at about 28.70 MPa. The values decreased gradually up to 0.65 MPa at the top and bottom ends of the caving zone. Modeling result reveals that high differential stress values were concentrated in two locations in the model- (i) at the left ends of coal pillar and (ii) at the upper part of the coal pillar. At the left ends of the coal pillar, the value is about 12.80 MPa, whereas at the upper part of the coal pillar, which is located between two caving zones, the value is 19.20 MPa. At the roof of the caving zone, the differential stress value ranges from 3.20 to 6.40 MPa (Fig. 4c). Fig. 5a shows the distribution contours of total displacement after development of two caving zones due to ignition. The simulation resulted in a total displacement of 0.150 m towards the roof, which gradually reduced to 0.30 m towards the upper part of the model. Displacement values decreased gradually from the caving zone to the upper interior of the overburden rock strata.

The absolute vertical displacement around the two caving zones is illustrated in Fig. 5b. A vertical displacement of about 0.120 m was simulated at the immediate roof of the left caving zone, whereas the value was 0.130 m at the immediate roof of the right caving zone. The absolute horizontal displacement around the two caving zones is illustrated in Fig. 5c. A horizontal displacement value in the model ranges from 0.00 m to 0.030 m. At the immediate roof of the left caving zone, the value was simulated of about 0.022 m, whereas the value ranges from 0.002 m to 0.020 m at the immediate roof of the right caving zone (Fig,. 5c). The distribution contours of the strength factor (Fig. 6) values ranged from 0.86 to 1.29 around the caving zone. A strength factor value of about 1.29 was simulated at the immediate roof of the coal pillar, whereas the value was 1.71 at the bottom of the coal pillar.

6. DISCUSSIONS AND CONCLUSIONS

During underground coal gasification in any coal deposits, a cavity is formed as the coal burns and the roof collapses. Cavity results in lateral growth and is allowed to continue until the product gas quality deteriorates. The greater the lateral growth, the longer the life of a gasifier and the more cost-effective the operation[25]. Cavity will cause stress redistribution in the surrounding rocks and lead to a series of mechanical effects including rock movement, deformation and failure [21]. In the present FEM numerical simulation, we simulated in-situ stress patterns around cavity, displacements and failure tendency of rock strata in terms of strength factor. Our numerical modeling results reveal that the maximum value of the major principal stress (σ_1) is about 56.90 MPa at the bottom of the coal pillar, whereas the value is about 19.30 MPa at the upper part of the coal pillar. The minimum values of major principal (σ_1) stress range from 4.05 to 7.10 MPa and 7.10 MPa, at the middle upper part and bottom of the cavity, respectively (Fig. 4a). Our modeling results emphasize that the maximum values of major principal stress are highly concentrated in and around the coal pillar rather than that of roof and floor of cavity. Moreover, maximum values of total displacement (0.150 m), vertical displacement (0.120 m), horizontal displacement (0.030 m) and deformation vectors associated with 250 m width and 36 m height of cavity imply that the lateral growth will sustain for a reasonable time, which will enhance the long life of a gasifier.

In our modeling, simulated strength factor value associated with the immediate roof of two cavities ranges from 1.71 to 2.14. Major and minor principal stresses (σ_1 and σ_3) have an influence on the strength factor. In the case of elastic materials, the strength factor can be less than unity, since overstressing is allowed. If the strength factor is greater than 1, this indicates that the material strength is greater than the induced stress. If the strength factor is less than 1, this indicates that the stress in the material exceeds the material strength (i.e. the material

would fail) (https://www.rocscience.com). In the present numerical modeling, strength factor from 1.71 to 2.14 at the immediate roof of the caving imply that the overburden strata strength is good enough to enhance the lateral growth of a gasifier and facilitate the cost-effective operation.

ACKNOWLEDGEMENTS

The Ministry of Education of Bangladesh is greatly acknowledged for its financial support of research project No**. PS2016125**.

REFERENCES

[1] Huang, W.G., Wang, Z.T., Xin, L., Duan, T.H., Kang, G.J., 2012. Feasibility study on underground coal gasification of No. 15 seam in Fenghuangshan Mine. The Journal of The Southern African Institute of Mining and Metallurgy. Vol. 112, 897-903.

[2] Liang, J., Yu, C., and Yang, L.H. 1996. Feasibility study on underground coal gasification in Fuxin mine area. *Journal of Fuxin Mining Institute* (Natural Science), vol. 15, no. 3, 375-78.

[3] Bhutt, A.,W., Bazmi, A.,A., Zahedi,G., 2013. Underground coal gasification: From fundamentals to applications. Progress in Energy and Combustion Science Volume 39, Issue 1, February 2013, Pages 189-214.

[4] Burton, E., Friedmann, J., Upadhye, R., 2006. Best practices in underground coal gasification, draft. US DOE Contract No W-7405-Eng-48, Lawrence Livermore National Laboratory, Livermore, CA, USA (2006).

[5] Couch, G.R., 2009. Underground Coal Gasification. IEA Clean Coal Center, International Energy Agency, London (2009). (ISBN 978-92-9029-471-9).

[6] Najafi, Mehdi., Jalali, S., M., E., Kakaie, R., K., 2014. Thermal–mechanical–numerical analysis of stress distribution in the vicinity of underground coal gasification (UCG) panels. International Journal of Coal Geology 134–135, 1-16.

[7] Orlov, G.V., 2018. The effects of rock deformation in underground coal gasification. Underground Coal Gasification and Combustion. 2018, Pages 283-327.

[8] Stuermer, D.H., Ng, D.J., Morris, C.J., 1982. Organic contaminants in groundwater near an underground coal gasification site in northeastern Wyoming. Environ Sci Technol, 16 (9), 582-587.

[9] Wong, F.T., Mead, S.W., 1982. Water quality monitoring at the Hoe Creek test site: review and preliminary conclusions. Underground gasification: the state of the art. AIChE Symp, 79 (226),154-173.

[10] Walker, L., 1999. Underground coal gasification. Austr Coal Rev. 10 19-21.

[11] Kostur, K., Sasvari, T., 2010. Research of lignite underground gasification. Acta Montanistica Slovaca, 15 (2), 121-133.

[12] Drzewiecki, J., 2012. The basic technological conditions of underground coal gasification (UCG). AGH J Min Geoeng, 36 (1), 117-124.

[13] Lari, S., Courtney, R., Mostade, M., 2013. Underground coal gasification. The coal handbook. Towards cleaner production, Vol. 1 Production, Woodhead Pub. (2013), pp. 226-239.

[14] Palarski, J. Strozik, G., 2013. Reduction of environmental impacts from underground coal gasification by the use of backfilling of underground voids. Pregl. Górn. 1, 156-162.

[15] Bahl, S., Barbero, G., Hwang, J. J., Miklova, B., 2014. Underground coal gasification. NTNU Norvegian Univ. of Science a. Tecnnol. (2014). TPG41400 Natural Gas.

[16] Nieć, M., Sermet, E., Chećko, J., Górecki, Jerzy., 2017. Evaluation of coal resources for underground gasification in Poland. Selection of possible UCG sites. Fuel 208, 193-202.

[17] Volodymyr S. Falshtynskyi, Roman O.Dychkovskyi, Vasy G. Lozynskyi, Pavlo B. Saik., 2013. Determination of the Technological Parameters of Borehole Underground Coal Gasification for Thin Coal Seams. Journal of Sustainable Mining 12, Issue 3, 2013, Pages 8-16.

[18] Islam, M.R., Islam, M.S., 2005. Water inrush hazard in Barapukuria coal mine, Dinajpur District, Bangladesh. Bangladesh Journal of Geology 24, 1–17.

[19] Islam, M.R., Hayashi, D., 2008. Geology and coal bed methane resource potential of the Gondwana Barapukuria Coal Basin, Dinajpur, Bangladesh. International Journal of Coal Geology 75, 127–143.

[20] Islam, M.R., Hayashi, D., Kamruzzaman, A.B.M., 2009. Finite element modeling of stress distributions and problems for multi-slice longwall mining in Bangladesh, with special reference to Barapukuria coal mine. International Journal of Coal Geology 78(2), 91–109.

[21] Islam, M.R., and Shinjo, R., 2009a. Mining-induced fault reactivation associated with the main conveyor belt roadway and safety of Barapukuria Coal Mine in Bangladesh: Constraints from BEM simulations. International Journal of Coal Geology 79(4), 115-130.

[22] Islam, M.R., and Shinjo, R., 2009b. Numerical simulation of stress distributions and displacements around an entry roadway with igneous intrusion and potential sources of seam gas emission of Barapukuria coalmine, NW Bangladesh. International Journal of Coal Geology 78(4),249–262.

[23] Islam, M. R., Hye, M. A., and Faruque, M. O., 2018. Rockburst hazard and gas emission potential around an LTCC mining panel associated with a dyke and a fault affected zone of Barapukuria Coal mine in Bangladesh: A numerical modeling approach. Electronic Journal of Geotechnical Engineering, 2018 (23.02), pp 217-242.

[24] Wardell Armstrong, 1991, Techno-Economic Feasibility Study of Barapukuria Coal Project (unpubl.), Dinajpur, Bangladesh.

[25] Creedy, D. P., Garner, K., Holloway, S., Jones, N., and Ren, T. X., 2001. Review of Underground Coal Gasificatio Technological Advancements. Report No. COAL R211 DTI/Pub URN 01/1041

[26] Brady, B. H. G., and Brown, E. T., 2004. Rock Mechanics for underground mining. 2004. eBook ISBN: 1-4020-2116-X. p. 647.

[27] Zienkiewicz, O. C. (1977) The Finite Element Method, 3rd edn. McGraw-Hill: London.

[28] www.rocscience.com

APPENDIX

GOVERNING EQUATIONS

The differential equations of equilibrium in two dimensions for zero body forces [26] are

$$\frac{\partial \sigma_{xx}}{\partial x}+\frac{\partial \sigma_{xy}}{\partial y}=0, \quad \frac{\partial \sigma_{xy}}{\partial x}+\frac{\partial \sigma_{yy}}{\partial y}=0 \tag{1}$$

$$\text{or } \frac{\partial^2 \sigma_{xy}}{\partial x \partial y}=-\frac{\partial^2 \sigma_{xx}}{\partial x^2}=-\frac{\partial^2 \sigma_{yy}}{\partial y^2} \tag{2}$$

Strains for plane strain conditions and isotropic elasticity are given by

$$\varepsilon_{xx}=\frac{1}{E'}\left(\sigma_{xx}-\nu'\sigma_{yy}\right)$$

$$\varepsilon_{yy}=\frac{1}{E'}\left(\sigma_{yy}-\nu'\sigma_{xx}\right) \tag{3}$$

$$\gamma_{xy}=\frac{1}{G}\sigma_{xy}=\frac{2(1+\nu')}{E'}\sigma_{xy}$$

where $E'=\frac{E}{1-\nu^2}, \nu'=\frac{\nu}{1-\nu}$.

The strain compatibility equation in two dimensions is defined by

$$\frac{\partial^2 \varepsilon_{yy}}{\partial x^2}+\frac{\partial^2 \varepsilon_{xx}}{\partial y^2}=\frac{\partial^2 \gamma_{xy}}{\partial x \partial y} \tag{4}$$

Applying the expressions for the strain components in equation(4), then equation (2) produces

$$\frac{1}{E'}\left(\frac{\partial^2 \sigma_{yy}}{\partial x^2}-\nu'\frac{\partial^2 \sigma_{xx}}{\partial x^2}\right)+\frac{1}{E'}\left(\frac{\partial^2 \sigma_{xx}}{\partial y^2}-\nu'\frac{\partial^2 \sigma_{yy}}{\partial y^2}\right)=\frac{2(1+\nu')}{E'}\frac{\partial^2 \sigma_{xy}}{\partial x \partial y}=-\frac{(1+\nu')}{E'}\left(\frac{\partial^2 \sigma_{xx}}{\partial x^2}+\frac{\partial^2 \sigma_{yy}}{\partial y^2}\right)$$

which becomes, after simplification,

$$\frac{\partial^2 \sigma_{xx}}{\partial x^2}+\frac{\partial^2 \sigma_{xx}}{\partial y^2}+\frac{\partial^2 \sigma_{yy}}{\partial x^2}+\frac{\partial^2 \sigma_{yy}}{\partial y^2}=0$$

$$\left(\frac{\partial^2}{\partial x^2}+\frac{\partial^2}{\partial y^2}\right)\left(\sigma_{xx}+\sigma_{yy}\right)=0 \tag{5}$$

Equation (5) shows that the two-dimensional stress distribution for isotropic elasticity is independent of the elastic properties of the medium and that the stress distribution is the same for plane strain as for plane stress. The problem reduces to solving equations (1) and (5) subject to the imposed boundary conditions by employing Finite element Method [26].

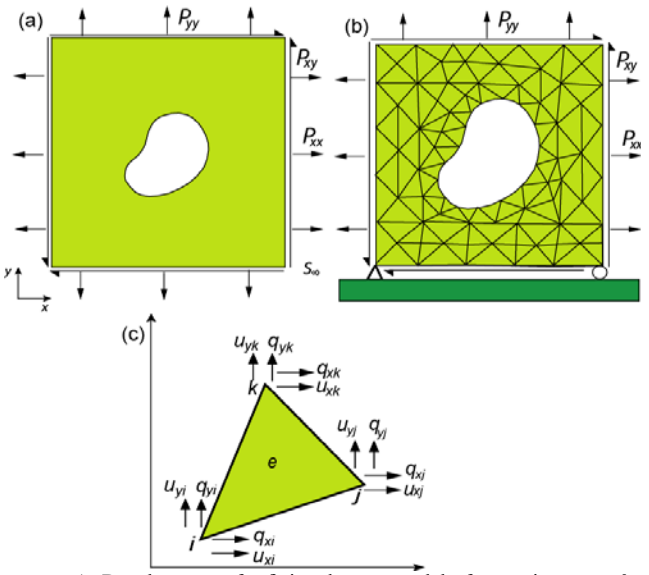

Figure 1A. Development of a finite element model of a continuum problem, and specification of element geometry and loading for a constant strain, triangular finite element.

THE FINITE ELEMENT METHOD

The foundation of the finite element method is the description of a problem domain surrounding an excavation, and decomposition of the domain into an assembly of discrete, interacting elements [26]. The cross-section of an underground opening generated in an infinite body subject to initial stresses p_{xx}, p_{yy}, p_{xy} is shown in Figure 1A(a). In Figure 1A(b), the selected boundary of the problem domain is shown, and appropriate supports and conditions are stipulated at the arbitrary outer boundary to make the problem statically stable. The domain has been decomposed into a set of triangular elements. A typical element of the set is exhibited in Figure 1A(c), with the points i, j, k defining the nodes of the element. The solution procedure described here is based on that by Zienkiewicz [27]. Displacement formulation of the finite element method starts with selection of a set of functions which describe the displacement components at any point within a finite element, in terms of the nodal displacements. The solution procedure then evolves from the imposed displacement field. Hence, the imposed displacement variation specifies the state of strain throughout an element because strain components are expressed uniquely in terms of various derivatives of the displacements.

These induced strains and the elastic properties of the medium together assess the induced stresses in an element. The initial stresses in combination with the induced stresses produce total stresses in the element. In the finite element method, transmission of internal forces between the edges of adjacent elements can be replaced by interactions at the nodes of the elements.

It is therefore essential to ascertain expressions for nodal forces which are statically equivalent to the forces acting between elements along the respective edges. Thus the procedure attempts to analyse the continuum problem (Figure 1A,a) in terms of sets of nodal forces and displacements for the discretised domain (Figure 1A,b). The solution procedure described here, exploits triangular element geometry, linear variation of displacement with respect to element intrinsic co-ordinates, and resultant constant stress within an element.

DISPLACEMENT VARIATION

In Fig 1A(c), $u_{xi}, u_{yi,}$ etc. are induced nodal displacements and displacements $[\mathbf{u}]$ at any point inside the element are to be evaluated by a suitable interpolation from the nodal values. A suitable interpolation formula using $[\mathbf{N}]$ as a matrix of interpolation functions is

$$[\boldsymbol{u}]=\begin{bmatrix}u_x\\u_y\end{bmatrix}=\sum[\mathbf{N}_i][\mathbf{u}_i]=\begin{bmatrix}\bar{\mathbf{N}}_i & \bar{\mathbf{N}}_j & \bar{\mathbf{N}}_k\end{bmatrix}\begin{bmatrix}\mathbf{u}_i\\\mathbf{u}_j\\\mathbf{u}_k\end{bmatrix}$$

$$=[\mathbf{N}][\mathbf{u}^e] \tag{6}$$

where $[\mathbf{u}_i]=\begin{bmatrix}u_{xi}\\u_{yi}\end{bmatrix}, [\mathbf{N}_i]=\bar{\mathbf{N}}_i=\begin{bmatrix}N_i & 0\\0 & N_i\end{bmatrix}$.

The terms N_i are stipulated functions of position, and $[\mathbf{u}^e]$ is a column vector listing the nodal displacements $u_{xi}, u_{yi,} u_{xj}, \cdots$ etc.

The interpolation functions must be chosen to obtain the nodal displacements at each node. This needs $[\mathbf{N}_i]_{xi,yj}=[\mathbf{I}]$, $[\mathbf{N}_i]_{xi,yi}=[\mathbf{0}]$, etc. It is obvious that $[\mathbf{N}_i]=N_i[\mathbf{I}]$ where N_i is a scalar function of position inside the element. A basic construction of a linear interpolation function is shown by expressing the displacements in terms of linear functions of position, i.e.

$$u_x=\alpha_1+\alpha_2 x+\alpha_3 y, u_y=\alpha_4+\alpha_5 x+\alpha_6 y \tag{7}$$

The six interpolation constants are obtained by letting the displacements take the nodal values when nodal coordinates are put in equation (7). Thus $\alpha_1, \alpha_2, \alpha_3$ are obtained by solving the simultaneous equations

$u_{xi}=\alpha_1+\alpha_2 x_i+\alpha_3 y_i, u_{xj}=\alpha_1+\alpha_2 x_j+\alpha_3 y_j, u_{xk}=\alpha_1+\alpha_2 x_k+\alpha_3 y_k$. Solution for $\alpha_1, \alpha_2, \alpha_3$ and some simplification yiels

$$u_x=\frac{1}{2\Delta}\left[(a_i+b_i x+c_i y)u_{xi}+\left(a_j+b_j x+c_j y\right)u_{xj}+ak+bkx+ckyuxk\right. \tag{8}$$

where $a_i = x_j y_k - x_k y_j, b_i = y_{j-} y_k, c_i = x_k - x_j$ with cyclic permutation of i, j, k to determine a_j, etc., and $2\Delta = 2\times$ area of the triangular element $= 2\begin{bmatrix} 1 & x_i & y_i \\ 1 & x_j & y_j \\ 1 & x_k & y_k \end{bmatrix}$. Solution for $\alpha_4, \alpha_5, \alpha_6$ produces an interpolation function for u_y similar to equation (8). The variation of displacements throughout an element is therefore expressed by

$$[\boldsymbol{u}] = \begin{bmatrix} u_x \\ u_y \end{bmatrix} = [\boldsymbol{N}][\mathbf{u}^e] = [N_i\mathbf{I}, N_j\mathbf{I}, N_k\mathbf{I}][u^e], \quad (9)$$

where $N_i = (a_i + b_i x + c_i y)/2\Delta$, etc.

When the displacement field in an element is obtained, the state of strain can be found from the strain-displacement relations. A strain vector for plane strain problems may be defined by

$$[\varepsilon] = \begin{bmatrix} \varepsilon_{xx} \\ \varepsilon_{yy} \\ \gamma_{xy} \end{bmatrix} = \begin{bmatrix} \frac{\partial u_x}{\partial x} \\ \frac{\partial u_y}{\partial y} \\ \frac{\partial u_x}{\partial y} + \frac{\partial u_y}{\partial x} \end{bmatrix} = \begin{bmatrix} \frac{\partial}{\partial x} & 0 \\ 0 & \frac{\partial}{\partial y} \\ \frac{\partial}{\partial y} & \frac{\partial}{\partial x} \end{bmatrix} \begin{bmatrix} u_x \\ u_y \end{bmatrix}$$

or $[\varepsilon] = [\mathbf{L}][\mathbf{u}]$ (10)

Using displacement equation (9), equation (10) becomes

$$[\varepsilon] = [\mathbf{L}][\boldsymbol{N}][\boldsymbol{u}^e] = [\mathbf{B}][\boldsymbol{u}^e]$$

where

$$[\mathbf{B}] = \begin{bmatrix} \frac{\partial N_i}{\partial x} & 0 & \frac{\partial N_j}{\partial x} & 0 & \frac{\partial N_k}{\partial x} & 0 \\ 0 & \frac{\partial N_i}{\partial y} & 0 & \frac{\partial N_j}{\partial y} & 0 & \frac{\partial N_k}{\partial y} \\ \frac{\partial N_i}{\partial y} & \frac{\partial N_i}{\partial x} & \frac{\partial N_j}{\partial y} & \frac{\partial N_j}{\partial x} & \frac{\partial N_k}{\partial y} & \frac{\partial N_k}{\partial x} \end{bmatrix}$$

The terms $\frac{\partial N_i}{\partial x}$, etc., of the matrix **B** are constant for linear displacement variation, and hence the strain components are invariant over the element.

PRINCIPAL STRESSES (Σ_1 AND Σ_3) IN 2D FEM MODELING

The present FEM modeling is related to plane strain conditions. For the case of plane strain condition, the principal stresses are defined in terms of in plane stress (σ_1 and σ_3) and out of plane stress (σ_z). The σ_1 option will plot contours of the major in-plane principal stress. The σ_3 option will plot contours of the minor in-plane principal stress. The σ_z option will plot contours of the out-of-plane principal stress. In two dimensions there are two principal stresses, which are the major principal stress and the minor principal stress. The major and minor principal stresses (σ_1 and σ_3) are expressed by the following equations (www.rocscience.com) –

σ_1 = major principal stress
σ_3 = minor principal stress

$$\sigma_1 = \frac{\sigma_y + \sigma_x}{2} + \sqrt{\left[\frac{\sigma_y - \sigma_x}{2}\right]^2 + \tau^2_{xy}}$$

$$\sigma_3 = \frac{\sigma_y + \sigma_x}{2} - \sqrt{\left[\frac{\sigma_y - \sigma_x}{2}\right]^2 + \tau^2_{xy}}$$

STRENGTH FACTOR USED IN RS2.9 SOFTWARE

The strength factor is calculated by dividing the rock strength by the induced stress at every point in the model mesh. All three principal stresses (σ_1, σ_3, and σ_z) have an influence on the strength factor. For the case of elastic materials, the strength factor can be less than unity, since overstressing is allowed. For the case of plastic materials, the strength factor is always greater than or equal to unity (https://www.rocscience.com). The strength factor represents the ratio of material strength to induced stress. A simple equation is-

$$\text{Strength factor} = \frac{S_{\max}}{S}$$

where $S_{\max}$ is the maximum strength of material, S is the induced stresses after underground excavation. Knowledge of the magnitudes of maximum strength of material and induced stress is an essential component of underground excavation design since, in many cases, the strength of the rock is exceeded and the resulting instability can have serious consequences on the behavior of the excavations. In *Slide2D*, Mohr-Coulomb failure criterion has been applied, where the failure criterion can be expressed as a function of three principal stress invariants as I_1, J_2 and J_3 [27].

$$I_1 = \sigma_{xx} + \sigma_{yy} + \sigma_{zz}$$

$$J_2 = \frac{1}{6}\left[(\sigma_{xx} - \sigma_{yy})^2 + (\sigma_{yy} - \sigma_{zz})^2 + (\sigma_{zz} - \sigma_{xx})^2\right] + \tau^2_{xy} + \tau^2_{yz} + \tau^2_{zx}$$

$$J_3 = \left(\sigma_{xx} - \frac{I_1}{3}\right)\left(\sigma_{yy} - \frac{I_1}{3}\right)\left(\sigma_{zz} - \frac{I_1}{3}\right) + 2\tau_{xy}\tau_{yz}\tau_{zx} - \left(\sigma_{xx} - \frac{I_1}{3}\right)\tau^2_{yz} - \left(\sigma_{yy} - \frac{I_1}{3}\right)\tau^2_{zx}$$

$$\theta = \frac{1}{3}\arcsin\left(-\frac{3\sqrt{3}J_3}{2J_2^{3/2}}\right), -\frac{\pi}{6} < \theta < \frac{\pi}{6}$$

$$S = \sqrt{J_2}$$

$$S_{\max} = \frac{\frac{I_1}{3}\sin\phi + c\cos\phi}{\cos\theta + \frac{\sin\theta\sin\phi}{\sqrt{3}}}$$

where, c = cohesion, ϕ = friction angle. A graphical representation of strength factor is given in Fig. 1B [28].

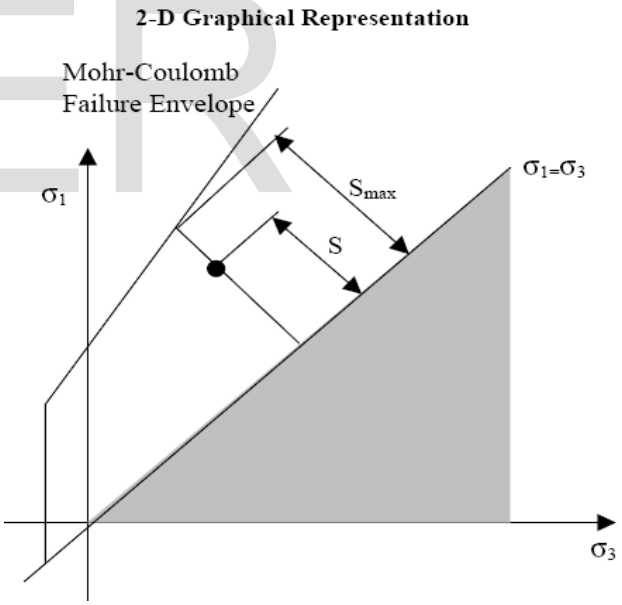

Figure 1B: A graphical representation of strength factor